Chinese Chemical Letters 31 (2020) 2077–2082

Contents lists available at ScienceDirect

Chinese Chemical Letters

journal homepage: www.elsevier.com/locate/cclet

Communication

Hierarchical $NiCo_2O_4$ microspheres assembled by nanorods with p-type response for detection of triethylamine

Chen Yang[a], Yongshan Xu[a], Lingli Zheng[a], Yingqiang Zhao[b], Wei Zheng[a], Xianghong Liu[a], Jun Zhang[a,*]

[a] College of Physics, Center for Marine Observation and Communications, Qingdao University, Qingdao 266071, China
[b] College of Chemistry, Chemical Engineering and Materials Science, Shandong Normal University, Ji'nan 250014, China

ARTICLE INFO

Article history:
Received 27 November 2019
Received in revised form 30 December 2019
Accepted 2 January 2020
Available online 9 January 2020

Keywords:
Microstructures
$NiCo_2O_4$
Metal oxide
p-type response
Gas sensor

ABSTRACT

The morphological and structural design provides an efficient protocol to optimize the performance of gas sensing materials. In this work, a gas sensor with high sensitivity for triethylamine (TEA) detection is developed based on p-type $NiCo_2O_4$ hierarchical microspheres. The $NiCo_2O_4$ microspheres, synthesized by a hydrothermal route, have a three-dimensional (3D) urchin-like structure assembled by nanorod building blocks. The structure-property correlation has been investigated by powder X-ray diffraction, X-ray photoelectron spectroscopy, transmission electron microscope, scanning electron microscope, N_2 adsorption-desorption tests and comprehensive gas sensing experiments. The influence of calcination temperature on the morphological structure and sensing performances has been investigated. Results reveal that the material annealed at 300 °C has a very large specific surface area of 125.27 m^2/g, thereby demonstrating the best TEA sensing properties including high response and low limit of detection (145 ppb), good selectivity and stability. The further increase of the calcination temperature leads to the collapse of the 3D hierarchical structure with significantly decreased surface area, which is found to decline the sensing performances. This work indicates the promise of ternary p-type metal oxide nanostructures for application in highly sensitive gas sensors.

Metal oxide semiconductors (MOSs) nanostructures have drawn enormous attention for gas sensors on account of their distinctive merits of low cost, portability, long-term stability, and environmental-friendliness [1,2]. Generally, these MOSs materials typically include ZnO [3,4], SnO_2 [5], NiO [6], WO_x [7–9], TiO_2 [10,11] and Fe_2O_3 [12,13] and significant progress has been made in the application of these binary MOSs as the sensor materials. Nevertheless, the binary MOSs still suffer from some shortcomings such as poor selectivity, relatively low sensitivity, and difficulty in regulating the sensing behaviors through tuning the cation sites [14]. Therefore, the design of ternary MOSs turns out to be an applicable method to develop advanced sensing materials to explore novel functionalities due to the benign synergic effect achieved by combining various metal oxide components [15–17].

An interesting and emerging class of ternary MOSs is cobalt-containing spinel oxides (MCo_2O_4, M = Ni, Zn, Cu), which have found widespread application in many important areas [18–20]. Among them, nickel cobalt oxide ($NiCo_2O_4$) with a p-type conductivity has been considered as a material with extensive prospects due to its outstanding properties such as high electronic conductivity, good structural stability, as well as high electrochemical activity [21]. Besides, it also offers notable advantages of multivalent traits facilitating redox reactions and outstanding catalytic activity for oxidation reactions due to their vast surface oxygen adsorption. Therefore $NiCo_2O_4$ has been extensively investigated in electrochemistry [21,22], while the capacity of this materials in gas sensor has been rarely explored. Gas sensing investigations of $NiCo_2O_4$ are carried out only in the very recent years. A few sensor reports of $NiCo_2O_4$ have demonstrated good response to ammonia, ozone and nitrogen oxide [23,24], while its potential in detecting triethylamine (TEA) has not been reported. TEA is a toxic organic compound, which is highly flammable and irritative. Exposure to TEA will do enormous harm to human health including serious skin corrosion and acute respiratory difficulty [25]. The European Commission has advocates a vocational exposure limit of 1 ppm (8 h time weighted average concentration (TWA)) for TEA for safety concern [26].

Herein, $NiCo_2O_4$ microspheres with a hierarchical structure are prepared by hydrothermal approach and researched as a p-type sensor material for TEA detection. The effect of calcination at

* Corresponding author.
E-mail address: jun@qdu.edu.cn (J. Zhang).

https://doi.org/10.1016/j.cclet.2020.01.011

varied temperatures on the structure and the sensing properties has been systematically studied. The $NiCo_2O_4$ microspheres annealed at 300 °C have a specific surface area of as large as 125.27 m^2/g, which demonstrates the best response for TEA. Increasing the annealing temperature is found to accelerate the response speed. The $NiCo_2O_4$ sensor also manifest quite good selectivity, low limit of detection (LOD), and excellent stability for TEA detection. Furthermore, the sensor response is shown to exhibit small decrease under a relative humidity below 75%.

In a typical synthesis process of $NiCo_2O_4$ hierarchical microspheres, 1.5 mmol $CoCl_2{\cdot}6H_2O$, 0.75 mmol $NiCl_2{\cdot}6H_2O$, and 45 mmol urea were separately dissolved in 20 mL ultrapure water by magnetic stirring at room temperature for 30 min. After that, the obtained solution was sealed in a 50 mL stainless-steel autoclave with Teflon-lined, which was kept at 120 °C for 6 h. The temperature of solution was dropt down to indoor temperature naturally when the reaction was over. Then the precipitate was swilled with ultrapure water and ethyl alcohol by centrifugation and desiccated at 60 °C for 12 h. Eventually, the as-synthesized precursor was annealed in air for 3 h at 300, 400 and 500 °C, respectively.

The crystalline phase of samples was identified by powder X-ray diffraction (XRD) analysis with Ni-filtered Cu Kα radiation (40 kV, 40 mA) on Rigaku Smartlab. The morphological structure were observed using scanning electron microscope (SEM, Zeiss sigma 300, German), transmission electron microscope (TEM, FEI JEM-2010) and high-resolution TEM (HRTEM) analyses. The surface chemical states were confirmed *via* X-ray photoelectron spectroscopy (XPS, Thermo ESCALAB 250, America) with the Al Kα anode of 1486.6 eV. The pore size distribution and the specific surface area were tested by N_2 adsorption-desorption experiments based on Brunauer-Emmet-Teller (BET) and Barrett-Joyner-Halenda (BJH) analysis using an ASAP 2060 at 77 K.

During the sensor prepared process, a small amount of the prepared samples was triturated in a mortar made of agate, then a spot of ultrapure water were dripped into to make a uniform slurry. Afterwards the slurry was uniformly smeared on a ceramic tube which is 4 mm long and 1 mm across to constitute a sensing membrane. A coil made by Ni-Cr alloy go through the ceramic tube to work as a heating unit and control the working temperature in the range of 60–300 °C by regulating the voltage. The prepared sensor (Fig. 1a) was installed on the experimental equipment (Fig. 1b) and went through a pilot run for more than 3 days before test. The response value (S) is defined as $S = R_a/R_g$ for oxidative gases and R_g/R_a for reductive gases. The R_a and R_g are the resistance of the sensors in air atmosphere and in target gas. The times of response and recovery are both defined as the time to attain 90% of the final signal. The relative humidity (RH) in the test chamber was tuned by introducing water vapor into the chamber and tested by an electronic humidity meter under ambient temperature (about 30 °C).

Fig. 2 displays the synthesis of $NiCo_2O_4$ microspheres. A hydrothermal approach is used to grow NiCo-containing microsphere precursor, which is converted to $NiCo_2O_4$ microspheres by thermal annealing. Depending on the annealing temperature, the microstructure of the final $NiCo_2O_4$ microspheres can be changed largely.

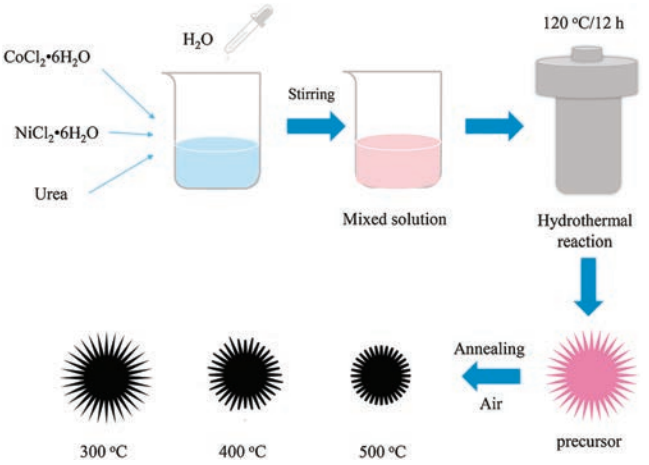

Fig. 2. The synthesis process of $NiCo_2O_4$ microspheres annealed at different temperature.

XRD analysis was carried out for identifying the crystallinity and purity of the $NiCo_2O_4$ micro-sphere calcined at 300, 400 and 500 °C, respectively. As displayed in Fig. 3a, all diffraction peaks can be vest in the spinel $NiCo_2O_4$ (JCPDF No. 73-1702) and no obvious diffraction from other crystalline phases can be detected, indicating the high purity of $NiCo_2O_4$. Fig. 3b displays the spinel structure of $NiCo_2O_4$. It is seen that Ni atoms are located in the octahedron and the Co atoms are embedded in both the octahedral and the tetrahedral sites, which form a 3D tunnel structure that is highly advantageous for gas diffusion [27].

As shown in Fig. 4, scanning electron microscopy (SEM) provides the morphological information of the $NiCo_2O_4$ microsphere annealed at different temperature. The SEM image of $NiCo_2O_4$ precursor (Fig. 4a) displays a stratified microspheres structure assembled by innumerable nanorods, which endows the microsphere with an enormous specific surface area and porous architecture. Fig. 4b reveals that the hierarchical microsphere morphology was well retained after annealing at 300 °C, revealing the superior structural stability of the microspheres. With the increase of calcination temperature to 400 °C, the urchin-like structure still can be observed in Fig. 4c, but the nanorods in the microsphere were partly devastated. When the calcination temperature increases to 500 °C, as displayed in Fig. 4d, the urchin-like structure of the microspheres was totally broken. The nanorods are absent and are transformed into nanoparticles due to the quite high annealing temperature. The detailed microstructure of $NiCo_2O_4$ microspheres annealed at 300 °C was further revealed by transmission electron microscopy (TEM) and high-resolution TEM (HRTEM). Figs. 4e and f show the morphology of

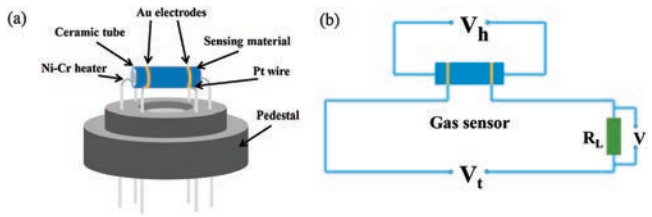

Fig. 1. (a) Diagrammatic drawing of the sensor facility. (b) The testing theory of the sensor testing device.

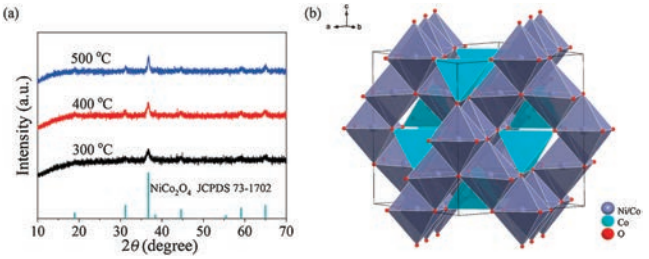

Fig. 3. (a) XRD patterns of $NiCo_2O_4$ microsphere calcined at different temperature. (b) The atomic structure of $NiCo_2O_4$.

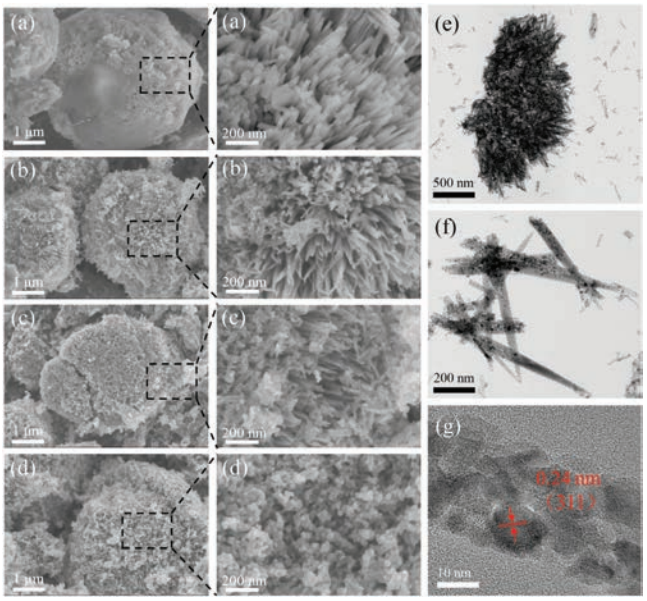

Fig. 4. The SEM images of (a) precursor; $NiCo_2O_4$ microspheres annealed at (b) 300, (c) 400 and (d) 500 °C. (e, f) TEM and (g) HRTEM images of $NiCo_2O_4$ microspheres annealed at 300 °C.

nanorod subunits detached from the $NiCo_2O_4$ microsphere. It can be seen that the nanorod subunits displays a porous characteristic, providing vast gas diffusion channels, which is beneficial for gas sensing [28,29]. Besides, the grain boundaries between the adjacent nanoparticles offer plentiful surface active sites for the adsorption and desorption of gases, which will efficaciously enhance the performances of gas sensing [30]. The HRTEM image shown in Fig. 4g displays the crystalline fringe with a calculated lattice spacing of 0.24 nm, which is consistent with the (311) plane of the cubic $NiCo_2O_4$ structure [31].

The XPS measurement was performed to demonstrate the surface chemistry of the $NiCo_2O_4$ microsphere annealed at 300 °C, and the results are presented in Fig. S1 (Supporting information). All the binding energies were corrected by referring to the C 1s peak at 284.8 eV of the surface adventitious carbon. The XPS survey shown in Fig. S1a manifests the presence of nickel, cobalt and oxygen elements. The Ni 2p spectrum can be well-fitted to two kinds of nickel species containing Ni^{3+} and Ni^{2+} together with two shakeup satellites (Fig. S1b). The two peaks at around 873.01 and 855.41 eV is attributed to Ni $2p_{1/2}$ and Ni $2p_{3/2}$ of Ni^{3+}, while the peak at 872.61 eV is attributed to Ni $2p_{1/2}$ of Ni^{2+} [32]. Moreover, the Co 2p spectrum can be fitted to two sets of cobalt species, which contains Co^{3+} and Co^{2+} (Fig. S1c). The two peaks at around 794.71 and 779.91 eV is attributed to Co $2p_{1/2}$ and Co $2p_{3/2}$ of Co^{3+}, while the other two peaks at 796.31 and 781.01 eV is attributed to Co $2p_{1/2}$ and Co $2p_{3/2}$ of Co^{2+} [33]. As displayed in Fig. S1d, the O 1s spectrum can be well-fitted into three oxygen components, consisting of the lattice oxygen species (O_{latt}), the primary component for O 1s, the adsorbed oxygen species (O_{ads}), which is take charge of the surface sensing reactions, as well as the adsorbed OH groups or molecular water (O_{surf}) [34].

N_2 adsorption-desorption experiments were executed to investigate the specific surface area and pore structure properties of $NiCo_2O_4$ microspheres and the results are presented in Fig. S2 (Supporting information). As stipulated by IUPAC classification, the N_2 adsorption-desorption isotherms of the precursor and the $NiCo_2O_4$ microspheres with H1-type hysteresis loop all can be categorized as type-IV curve, indicating the existence of mesoporous structure. Moreover, the hysteresis loop in isotherms of the $NiCo_2O_4$ microsphere annealed at 500 °C is not as obvious as the other three samples. This is mainly because the significantly larger pore diameter of the sample caused by the collapse of the 3D hierarchical structure under high temperature annealing. This also can be intuitively confirmed by the pore diameter distribution curves shown in the insert of Fig. S2. The BET surface areas, pore diameter distribution and pore volume were collated in Table S1 (Supporting information). The specific surface area of $NiCo_2O_4$ microsphere annealed at 300 °C have the highest value of 125.27 m^2/g, while the products annealed at 400 °C and 500 °C only have a value of 52.00 and 28.47 m^2/g, respectively, which is in accordance with the result of SEM that the urchin-like structure was broken at the high temperature.

Fig. 1 shows the scheme of the sensor device and test theory of the gas sensing test system. In general, the response of a resistive semiconductor gas sensor can be largely affrcted by the operating temperature. This is mainly due to the surface adsorption-desorption process and redox events are highly temperature-dependent [35]. Therefore, the responses of the gas sensor based on $NiCo_2O_4$ microspheres to 50 ppm TEA at different temperature were tested to confirm the optimum operating temperature. As displayed in Fig. 5a, the response of all gas sensors gradually increases to the maximum values and then decreases with the increase of operating temperature, showing a typical moutain-type shape. Therefore, the optimum operating temperature is determined to be 180 °C, and all other sensing performances were tested at 180 °C. The inferior response at relatively low temperatures might because lack of sufficient heat energy to initiate sensing reaction with the oxygen species absorbed on the surface. As the temperature increases, higher response appeared because of the higher reaction activity and the changeover of the oxygen species absorbed on the surface ($O_{2(ads)} \rightarrow O_2^-{}_{(ads)} \rightarrow O^-{}_{(ads)} \rightarrow O^{2-}{}_{(ads)}$). Nevertheless, with the temperature further increasing, the adsorption capacity of TEA molecules will be decreased, and sequentially reduce the amount of

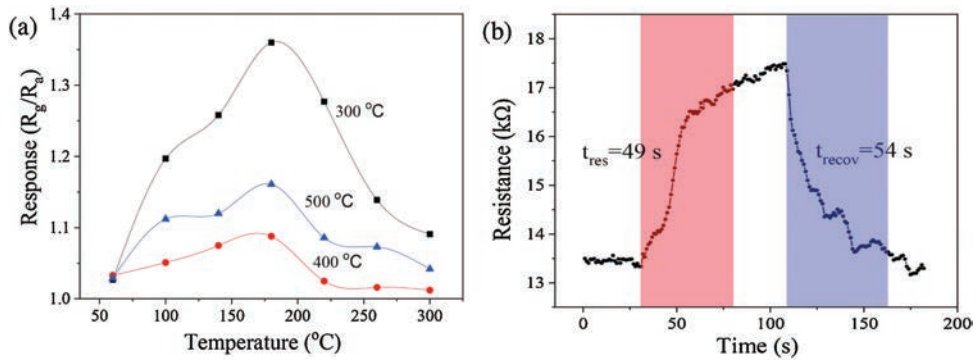

Fig. 5. (a) The response of $NiCo_2O_4$ microspheres at different temperature to 50 ppm TEA. (b) The resistance variation of $NiCo_2O_4$ microspheres annealed at 300 °C to 50 ppm TEA at 180 °C.

effective adsorption of TEA molecules, leading to the decrease of gas response eventually [16,36,37]. In addition, it is observed that the $NiCo_2O_4$ microsphere calcined at 300 °C exhibit the highest response among the three sensors. This is probably because of the excellent integrity of the hierarchical structure of the materials (Fig. 4b), which endows a high porous architecture and the very large specific surface area for molecule diffusion and adsorption. The response of products annealed at 500 °C is higher than that of calcined at 400 °C, which could be ascribed to the better crystallinity of the products under higher annealing temperature. The resistance variation of $NiCo_2O_4$ microspheres annealed at 300 °C to 50 ppm TEA is shown in Fig. 5b. An increase of sensor resistance is observed on exposure to TEA, which is typical of p-type semiconductor sensors. Besides, the response and recovery time are 49 s and 54 s, respectively, which is quite fast for a p-type semiconductor sensor.

The response behaviors of $NiCo_2O_4$ microspheres are further appraised by testing their response to different concentration of TEA ranging from 2 ppm to 500 ppm at 180 °C. As shown in Fig. 6a, a stepwise increase in the dynamic response-recovery curves can be ovserved along with the gradually increasing TEA concentration. Meanwhile, the $NiCo_2O_4$ microspheres annealed at 300 °C exhibit the highest response to each concentration. Response-recovery time is another key parameter for gas sensors during the actual application. Fig. 6b displays the response-recovery times on exposure to 500 ppm TEA at 180 °C. It is can be seen that the $NiCo_2O_4$ microsphere calcined at 500 °C exhibit the fastest response-recovery times (30 and 37 s) among the three sensors. This may be owing to the limited specific surface area of the products under highest annealing temperature.

The fitted sensor responses as a function of TEA concentration are shown in Fig. 6c. On the basis of the linear fitting analysis, the fitting line of $NiCo_2O_4$ microspheres annealed at 300 °C has a slope of *ca.* 0.063, which is higher than that of annealed at 400 °C (0.030) and 500 °C (0.027). This result exposits that the $NiCo_2O_4$ microsphere annealed at 300 °C has the highest sensitivity, which is due to the largest surface area and the unique porous structure. Thereupon, a lower limit of detection (LOD, calculated as $3\sigma/s$ [38]) of 145 ppb is calculated for $NiCo_2O_4$ microsphere annealed at 300 °C, in comparison to the 254 ppb of annealed at 400 °C and 180 ppb of annealed at 500 °C. Obviously the $NiCo_2O_4$ microspheres annealed at 300 °C manifest superior sensing performances over the counterparts annealed at 400 and 500 °C, with better response, higher sensitivity, and lower LOD at the sub-ppm level. Since selectivity is particularly significant for gas sensor, Fig. 6d shows the responses of $NiCo_2O_4$ microsphere annealed at 300 °C to 50 ppm various gases, including methanol, ethanol, butanol, acetone, trimethylamine, formaldehyde, H_2 and NO_2. It is obvious that the sensor shows the maximum response to TEA compared with other gases, indicating the excellent selectivity to TEA. Besides, stability and repeatability are also vital parameters for the practical use of gas sensor. Fig. 6e displays the periodic response and recovery of the sensor based on $NiCo_2O_4$

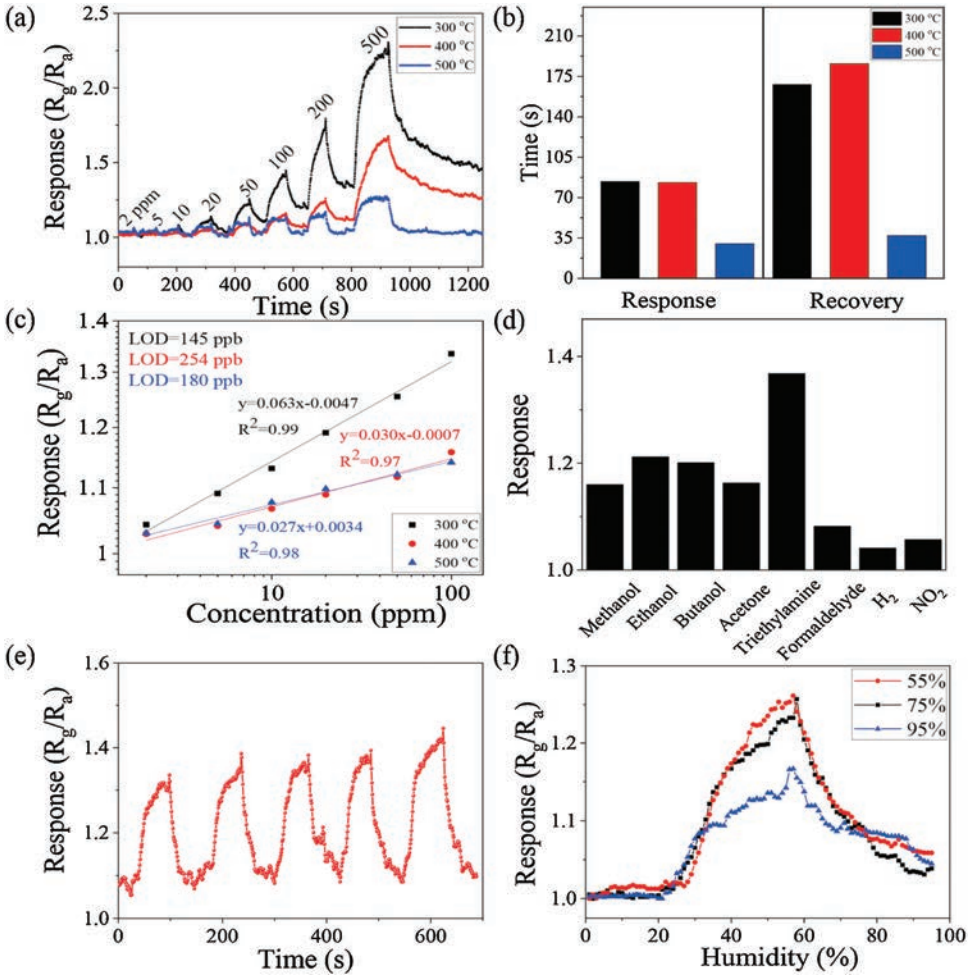

Fig. 6. (a) The sensing transients to different concentration of TEA. (b) The response and recovery times to 500 ppm TEA. (c) The fitted function of TEA concentration of the $NiCo_2O_4$ microspheres annealed at 300, 400 and 500 °C. (d) Sensor response of $NiCo_2O_4$ microsphere annealed at 300 °C to 50 ppm different gases. (e) The stability of the sensor to 50 ppm TEA. (f) Sensors response of as-prepared samples to 50 ppm TEA in different humidity environment. All of these tests were performed at 180 °C.

microspheres annealed at 300 °C on exposure to 50 ppm TEA at 180 °C. It can be seen that there is almost no change during the five cycles of sensing test, which implies outstanding stability and reproducibility of the sensor. Humidity is another factor that must be considered in practical application of gas sensors. The control tests were carried out with 50 ppm TEA under the relative humidity (RH) of 55%, 75% and 95%. As displayed in Fig. 6f, the response shows a slight decrease with the increase of RH. This phenomenon has also been reported in n-type semiconductors gas sensor [39], which can be ascribed to the fact that the active sites for sensing reactions are occupied and the surface absorbed oxygen are eliminated by water adsorption in high humidity, resulting in the reduction of the effective absorption of target molecules.

As is widely accepted, the sensing mechanism of MOSs is based on the variation in resistance caused by surface adsorption and desorption of gas molecules during the sensing processes [2]. When the sensing materials contact with air (Fig. 7a), oxygen molecules will be adsorbed on the surface and chemisorbed oxygen species (O_2^-, O^- or O^{2-}) will come into being by capturing unbound electrons from the conduction band of the materials because of their large electronegativity [40]. The reaction can be expressed as reactions 1–4 [41]:

$$O_{2(g)} \rightarrow O_{2(ad)} \quad (1)$$

$$O_{2(ad)} + e^- \rightarrow O_2^-{}_{(ad)} \quad (2)$$

$$O_2^-{}_{(ad)} + e^- \rightarrow 2O^-{}_{(ad)} \quad (3)$$

$$O^-{}_{(ad)} + e^- \rightarrow O^{2-}{}_{(ad)} \quad (4)$$

For $NiCo_2O_4$, a typical p-type semiconductor, this electron-capture process would cause a decrease of electron concentration, causing the formation of hole accumulation layer (HAL) and lower resistance [42]. When reducing gas like TEA is introduced (Fig. 7b), the gas molecules will have reaction with the oxygen ions adsorbed on the surface by the following reaction (5) [7,43]:

$$N(C_2H_5)_3 + O^- \rightarrow NO_2 + H_2O + CO_2 + e^- \quad (5)$$

The electrons trapped by the chemisorbed oxygen species are released back to the materials, which make the HAL become thinner and leads to an increase of resistance. When the sensing materials are re-exposed to air atmosphere, the free electrons from the materials will be captured again by the re-adsorption of oxygen, which will decrease the resistance of the sensor again.

Therefore, the superior sensing performances of $NiCo_2O_4$ microsphere are mainly owing to the highly susceptive hierarchical micro/nanostructure, which can provide a considerable specific surface area and more active sites for molecule adsorption. In the same time, the porous structure could provide vast gas diffusion channels (Fig. 7), which can facilitate the gaseous diffusion and accelerate the mass transfer within the sensing layers.

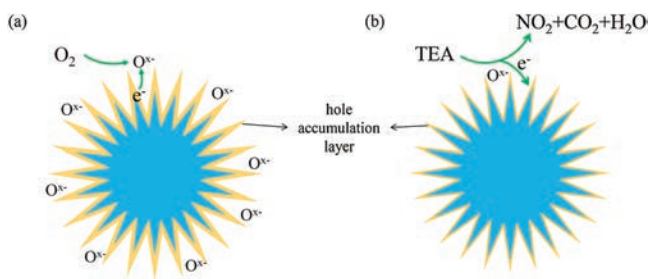

Fig. 7. The hole accumulation layer sensing mechanism of (a) $NiCo_2O_4$ microspheres in air, (b) $NiCo_2O_4$ microspheres in TEA.

In summary, hierarchical $NiCo_2O_4$ microspheres with a p-type response were synthesized and demonstrated for gas sensor application towards TEA detection. The $NiCo_2O_4$ microspheres with a very high specific surface area of 125.27 m^2/g exhibit superior selectivity to TEA, low LOD of 145 ppb and excellent stability. The unique hierarchical structure with large specific surface area accounts for the outstanding gas sensing performance by providing numerous surface active site. Furthermore, the significance of this unique structure for gas sensing was certified by increasing the annealing temperature to 400 °C and 500 °C, causing the destruction of hierarchical structure as well as the declined sensor responses. Our work indicates the importance of morphology design for developing p-type sensor materials, as well as the potential of the $NiCo_2O_4$ microspheres for TEA detection.

Declaration of competing interest

The authors declare that they have no known competing financial interests or personal relationships that could have appeared to influence the work reported in this paper.

Acknowledgments

This work is financially supported by the National Natural Science Foundation of China (Nos. 61971252, 51972182 and 21601098), Shandong Provincial Science Foundation (Nos. ZR2019BF008 and ZR2017JL021) and Key Research and Development Program (No. 2018GGX102033).

Appendix A. Supplementary data

Supplementary material related to this article can be found, in the online version, at doi:https://doi.org/10.1016/j.cclet.2020.01.011.

References

[1] X. Liu, T. Ma, N. Pinna, J. Zhang, Adv. Funct. Mater. 27 (2017) 1702168.
[2] J. Zhang, X. Liu, G. Neri, N. Pinna, Adv. Mater. 28 (2016) 795–831.
[3] F.L. Meng, H.X. Zheng, Y.F. Sun, M.Q. Li, J.H. Liu, Sensors 17 (2017) 1478.
[4] Y. Su, G. Xie, H. Tai, et al., Nano Energy 47 (2018) 316–324.
[5] X. Liu, T. Ma, Y. Xu, et al., Sens. Actuator. B –Chem. 264 (2018) 92–99.
[6] Y. Ren, X. Yang, X. Zhou, et al., Chin. Chem. Lett. 30 (2019) 2003–2008.
[7] Y. Xu, T. Ma, Y. Zhao, et al., Sens. Actuator. B –Chem. 300 (2019) 127042.
[8] T. Li, Y. Shen, S. Zhao, et al., Ceram. Int. 44 (2018) 4814–4823.
[9] J. Ma, Y. Ren, X. Zhou, et al., Adv. Funct. Mater. 28 (2018) 1705268.
[10] Z. Ye, H. Tai, T. Xie, et al., Sens. Actuator. B –Chem. 223 (2016) 149–156.
[11] C. Wang, Y. Li, P. Qiu, et al., Chin. Chem. Lett. 31 (2020) 1119–1123.
[12] T. Ma, L. Zheng, Y. Zhao, et al., ACS Appl. Nano Mater. 2 (2019) 2347–2357.
[13] X. Wang, T. Wang, G. Si, et al., Sens. Actuator. B –Chem. 302 (2020) 127165.
[14] T. Zhou, S. Cao, R. Zhang, et al., ACS Appl. Mater. Interfaces 11 (2019) 28023–28032.
[15] X. Zhou, W. Feng, C. Wang, et al., J. Mater. Chem. A 2 (2014) 17683–17690.
[16] X. Zhou, J.Y. Liu, C. Wang, et al., Sens. Actuator. B –Chem. 206 (2015) 577–583.
[17] T. Zhou, X. Liu, R. Zhang, Y. Wang, T. Zhang, Sens. Actuator. B –Chem. 290 (2019) 210–216.
[18] G.Y. Zhang, B. Guo, J. Chen, Sens. Actuator. B –Chem. 114 (2006) 402–409.
[19] S. Vijayanand, P.A. Joy, H.S. Potdar, D. Patil, P. Patil, Sens. Actuator. B –Chem. 152 (2011) 121–129.
[20] X.Y. Yu, X.Z. Yao, T. Luo, et al., ACS Appl. Mater. Interfaces 6 (2014) 3689–3695.
[21] C. Guan, X.M. Liu, W.N. Ren, et al., Adv. Energy Mater. 7 (2017) 1602391.
[22] S. Zhu, J.J. Li, X.Y. Deng, et al., Adv. Funct. Mater. 27 (2017) 1605017.
[23] A. Sharma, P. Bhojane, A.K. Rana, Y. Kumar, P.M. Shirage, Scripta Mater. 128 (2017) 65–68.
[24] N. Joshi, L.F. da Silva, H. Jadhav, et al., RSC Adv. 6 (2016) 92655–92662.
[25] M. Bietti, M. Salamone, Org. Lett. 12 (2010) 3654–3657.
[26] Y.S. Xu, T.T. Ma, L.L. Zheng, et al., Sens. Actuator. B –Chem. 284 (2019) 202–212.
[27] W.-w. Liu, C. Lu, K. Liang, B.K. Tay, J. Mater. Chem. A 2 (2014) 5100–5107.
[28] J. Qi, X.Y. Lai, J.Y. Wang, et al., Chem. Soc. Rev. 44 (2015) 6749–6773.
[29] X. Zhou, X. Cheng, Y. Zhu, et al., Chin. Chem. Lett. 29 (2018) 405–416.
[30] L. Wang, S. Chen, W. Li, et al., Adv. Mater. 31 (2019) 1804583.
[31] C. Ji, F. Liu, L. Xu, S. Yang, J. Mater. Chem. A 5 (2017) 5568–5576.
[32] R. Ding, L. Qi, M.J. Jia, H.Y. Wang, Nanoscale 6 (2014) 1369–1376.

[33] Y. Yang, D.H. Zeng, L. Gu, et al., Electrochim. Acta 286 (2018) 1–13.
[34] Q. Du, L. Wang, J. Yang, et al., Sens. Actuator. B –Chem. 273 (2018) 1786–1793.
[35] H. Gong, J.Q. Hu, J.H. Wang, C.H. Ong, F.R. Zhu, Sens. Actuator. B –Chem. 115 (2006) 247–251.
[36] X. Zhou, X.W. Li, H.B. Sun, et al., ACS Appl. Mater. Interfaces 7 (2015) 15414–15421.
[37] Y. Xu, T. Ma, L. Zheng, et al., Sens. Actuator. B –Chem. 288 (2019) 432–441.
[38] A. Shrivastava, V.B. Gupta, Chron. Young Sci. 2 (2011) 21.
[39] K. Wan, D. Wang, F. Wang, et al., ACS Appl. Mater. Interfaces 11 (2019) 45214.
[40] N. Barsan, U. Weimar, J. Electroceram. 7 (2001) 143–167.
[41] N. Zhang, S.P. Ruan, Y.Y. Yin, et al., ACS Appl. Nano Mater. 1 (2018) 4671–4681.
[42] H.J. Kim, J.H. Lee, Sens. Actuator. B –Chem. 192 (2014) 607–627.
[43] Y. Takao, M. Nakanishi, T. Kawaguchi, et al., Sens. Actuator. B –Chem. 25 (1995) 375–379.